Comparative study of ultraviolet detectors based on ZnO nanostructures grown on different substrates

H. I. Abdulgafour, Z. Hassan, N. M. Ahmed, and F. K. Yam

Citation: J. Appl. Phys. **112**, 074510 (2012); doi: 10.1063/1.4757619
View online: http://dx.doi.org/10.1063/1.4757619
View Table of Contents: http://jap.aip.org/resource/1/JAPIAU/v112/i7
Published by the American Institute of Physics.

Comparative study of ultraviolet detectors based on ZnO nanostructures grown on different substrates

H. I. Abdulgafour,[a] Z. Hassan, N. M. Ahmed, and F. K. Yam
Nano-Optoelectronics Research Laboratory, School of Physics, Universiti Sains Malaysia, 11800 Penang, Malaysia

(Received 21 February 2012; accepted 29 August 2012; published online 9 October 2012)

Pd/ZnO/Pd metal-semiconductor-metal photodetectors have been successfully fabricated using a variety of high-quality ZnO nanostructures. The nanostructures used included well-aligned nanorods, tetrapod-like nanorods, and hair-like nanowires and were synthesized on Si (100), porous silicon (PS/Si), and quartz substrates, respectively, using a catalyst-free vapor–solid mechanism for comparison. The morphological, structural, and optical properties of these nanostructures were investigated. Upon illumination with ultraviolet light (365 nm), the responsivity values of the fabricated photodetectors on PS/Si, Si, and quartz substrates were 0.22, 0.073, and 0.053 A/W, which correspond to quantum efficiencies of 85%, 28%, and 20%, respectively, at an applied bias of 5 V. The present study demonstrated that ZnO nanowires/PS exhibited a relatively fast photoresponse, with a rise time of 0.089 s and fall time of 0.085 s. The ZnO nanorods/Si and ZnO nanotetrapods/quartz exhibited a slow response, with rise times of 0.128 and 0.194 s and fall times of 0.362 and 0.4 s, respectively. The study suggests that the response time of the ZnO nanostructures to ultraviolet exposure is dependent on the type of substrate used. Results show that these nanostructures are suitable for sensing applications. © *2012 American Institute of Physics*. [http://dx.doi.org/10.1063/1.4757619]

I. INTRODUCTION

ZnO, a II–VI compound semiconductor, is one of the most prominent semiconductors in the metal-oxide family. ZnO has a stable wurtzite structure with lattice spacing *a* of 0.325 nm and *c* of 0.521 nm. It has a wide bandgap of 3.37 eV and a high exciton binding energy of 60 meV, which ensures an efficient excitonic ultraviolet (UV) emission at room temperature. ZnO is bio-safe, biocompatible, and can be directly used for biomedical applications without coatings.[1] The literature illustrates the key roles that one-dimensional (1D) ZnO nanostructures play in nanoscience and nanotechnology development. Growing interests in the synthesis of ZnO nanostructures are caused by promising applications in nanoscale technologies and devices.

Recently, quasi-1D ZnO nanostructures such as nanowires (NWs),[2,3] nanorods,[4] and nanobelts[5] have attracted great interest. These nanostructures show potential applications in optoelectronics, chemical sensors, and UV detectors because of their unique electrical and photonic properties. 1D ZnO nanostructures have been fabricated using various methods including thermal evaporation,[6] thermal chemical vapor deposition,[3] metalorganic chemical vapor deposition,[4] and sol–gel process.[7]

The vapor–liquid–solid process is commonly introduced to achieve vertically well-aligned ZnO NWs on several types of epitaxy substrates including sapphire,[8] GaN,[9] ZnO film-coated substrate,[10] SiC,[11] and Si substrate.[12] On the other hand, various nanoparticles or nanoclusters have been used as catalysts, such as Au,[13] Cu,[14] Co,[15] and Sn.[16]

In the vapor–solid (VS) process, the nanostructures are produced by direct condensation from the vapor phase. In a typical VS process, complex ZnO nanostructures, such as nanohelixes and nanobelts, have been synthesized by Kong and Wang.[17] Diverse ZnO nanostructures can be obtained using this method. The diversity and versatility of morphologies of ZnO are probably wider than any other materials known to date.[18,19] Furthermore, the conductance of ZnO NWs is extremely sensitive to UV light exposure. The light-induced conductivity enabled them to reversibly switch the nanowires between off and on states. When the NWs were exposed to 365 nm UV light, the NW photodetector exhibited strong power dependence and excellent wavelength selectivity.[20]

In the present work, we have successfully fabricated metal-semiconductor-metal (MSM) photodetectors on different substrates. High-quality ZnO nanostructures like nanorods, tetrapod-like nanorods, and hair-like NWs, which have been produced at a low cost were used. The fabrication was performed using a simpler route through the VS mechanism without a catalyst at 800 °C. Details of the ZnO nanostructure growth and the UV detector fabrication procedures, as well as the optical and electrical properties of the fabricated photodetectors, are presented in Sec. II.

II. EXPERIMENTAL DETAILS

A. Si and quartz substrate preparation

N-type silicon wafer with (100) orientation and quartz substrates were chosen as substrates and cut into (12×12) mm^2 pieces. Before ZnO nanostructures were grown, a 100 nm thick of SiO_2 was deposited on Si substrate by wet

[a]Email: hind_alshaikh@yahoo.com.

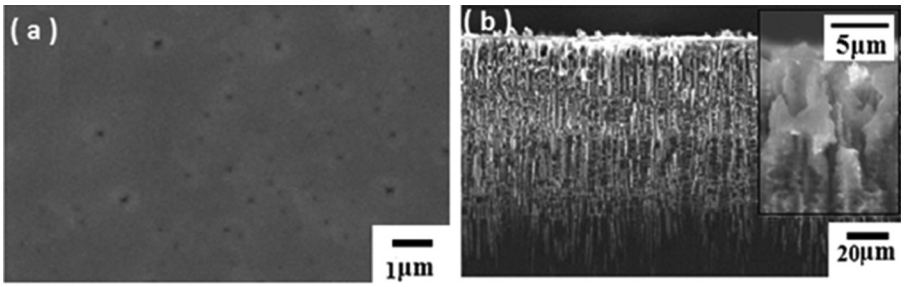

FIG. 1. (a) SEM image of PS sample and (b) SEM cross section of the PS sample prepared in 30 min etching time.

thermal oxidation in furnace at 1000 °C for 2 h. The substrates were ultrasonically cleaned with acetone and isopropyl alcohol and then rinsed with distilled water. The wafers were then dried using nitrogen gas to remove adsorbed dust and surface contamination.

B. Porous Si (PS/Si) preparation

The porous Si substrate was fabricated using the n-type Si (100) wafer through the electrochemical anodization method. A home-made Teflon cell was used for the process, and the Si sample and Pt wire were connected as anode and cathode, respectively. The electrolyte was composed of a mixture of 49% aqueous HF and 95% ethanol at a ratio of 1:4 by volume. For the electrochemical etching process, a constant current density (J) of 25 mA/cm^2 (supplied by a Keithley 220 programmable current source) was used for 30 min. After etching, the samples were rinsed with deionized water and dried in ambient air. Figure 1 shows the top-view SEM image of the PS sample prepared in 30 min etching time. A uniform distribution of pores at approximately 300 nm has been observed for PS samples prepared at optimized conditions.[21]

C. Synthesis of ZnO nanostructures

ZnO nanostructures were prepared in a horizontal tube furnace used for introducing gases at controlled rates. Different types of substrates were used, which include Si (100), PS/Si, and quartz, for ZnO nanostructure synthesis to investigate the effect of substrates on the properties of different ZnO nanostructures. Figure 2 shows the surface morphology of Si (100) and quartz substrates that used in our experiment. A series of experiments were performed for the different substrates under constant growth parameters.

Catalyst-free Zn metal powder (99.99% purity) was used to fabricate different types of ZnO nanostructures. The Zn powder was placed on a quartz boat inserted into the center of the horizontal tube furnace. The n-type (100) Si, quartz, and PS/Si substrates were ultrasonically cleaned before placing them at the top of the ceramic boat with the polished faces aligned toward the Zn powder. The boat was inserted after the tube furnace has reached the desired temperature. For the deposition in ambient wet oxygen (O_2), the gas was passed through bath water before being introduced into the furnace. The boat was then inserted into the center of the quartz tube furnace. The furnace was slowly heated from 420 °C to 800 °C under a continuous flow of highly pure argon and wet oxygen gases, with flow rates of (Ar) and (O_2) of 350 sccm and 126 sccm maintained for 1 h. After the evaporation, the alumina boat was slowly drawn out from the furnace and cooled down to room temperature.

D. UV photodetector fabrication and characterization

To fabricate the UV photodetectors, a Pd Schottky contact was deposited onto the surface of the different ZnO nanostructures as shown in Fig. 3. A 150 nm thick Pd contact was subsequently deposited onto the different substrates using a 150 W A500 Edwards RF magnetron sputtering unit, which served as electrode metal contacts. The fingers of the Pd contact electrodes were 0.23 mm wide and 4 mm long with 0.4 mm spacing. Each electrode consisted of four fingers for recording current–voltage (*I–V*) relationships at different bias voltages from 5 V to −5 V. The test fixture was connected with wires from the probes to the Keithley source unit to measure the *I–V* characteristics of the samples.

The surface morphology and structure of the ZnO nanostructures were examined using field-emission scanning electron microscopy (FE-SEM). A high-resolution x-ray diffractometer was used for phase identification. Optical properties were determined through photoluminescence (PL). The PL spectra of the ZnO nanostructures were obtained using a He–Cd laser with an excitation wavelength of 325 nm at room temperature. A Keithley electrometer (Model 6517A) was used to record the *I–V* characteristics. All the experiments in the current work were performed under atmospheric pressure and at room temperature.

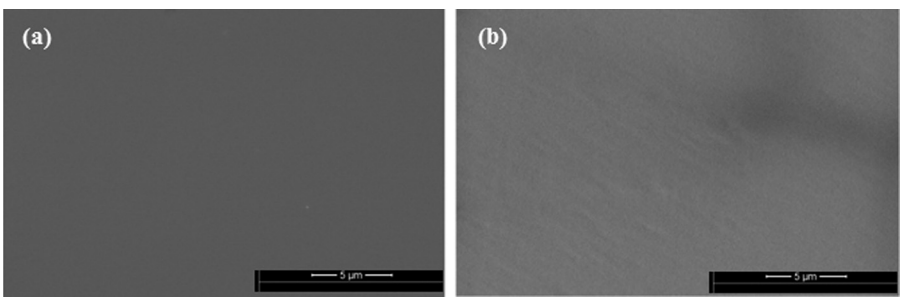

FIG. 2. (a) The SEM images (a) for Si and (b) for quartz substrates that used before growth ZnO nanostructures.

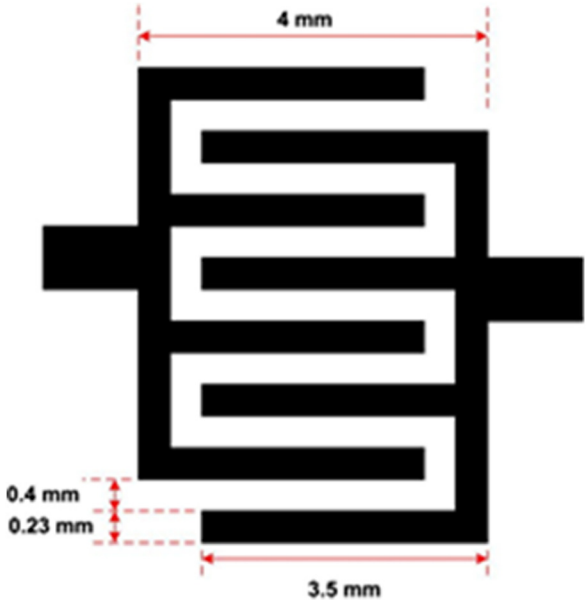

FIG. 3. Schematic diagram of the Pd Schottky contacts for ZnO MSM photodetector.

III. RESULTS AND DISCUSSION

A. Structural characteristics

ZnO nanostructures can be grown on three types of substrates (a) Si substrate, (b) PS/Si substrate, and (c) quartz substrate without using any metal catalyst. Figure 4 shows low- and high-magnification FE-SEM images of the ZnO nanostructures, which were grown on n-type Si, PS/Si, and quartz. The average diameter and length of the ZnO nanostructures were closely related to the substrate nature. The length, average diameter, and thickness of the nanostructures obtained on Si, PS/Si, and quartz substrates are 2.5 μm, 250 nm, and 5 μm; 7 nm, 85 μm, and 2 μm; and 3.5 μm, 125 nm, and 3 μm, respectively. In addition, the aspect ratios on the Si, PS/Si, and quartz were calculated as approximately 12, 28, and 82.3, respectively.

The average diameter of the NWs grown on the PS substrate was smaller than that of the nanorods grown on the Si substrate and the nano-tetrapods grown on the quartz substrate, as shown in Figs. 4(a2)–4(c2). The rough surface of the substrate obviously played an important role in controlling the initial stage of the ZnO nanostructure formation in the present case. The PS surface had a significant effect on the size and shape of the nanostructures; thus, there was a decrease in the length and size of the nanostructures based on the roughness of the surface morphology.[21]

The mechanism for the morphological evolution of the ZnO nanostructures synthesized in the present study is based primarily on surface diffusion. For bulk crystals, minimization of the surface energy is the driving force for the evolution of crystalline morphology. Hence, in equilibrium conditions, if there is no influence of epitaxy between the film and the substrate, the films exhibit self-texture and grow with a crystallographic plane of the lowest free energy (i.e., the plane with the closest packing of atoms and the highest reticular density) parallel to the surface.[22] We have found that morphological evolution for the ZnO film can be described by a mechanism mediated by surface diffusion.

Various ZnO nanostructures were formed on the different substrates positioned at the top of the source material. Nanostructures with different sizes were obtained for the different types of substrates because the supersaturation of ZnO vapor differed in these samples. Supersaturation is one of the key factors in determining the morphology of nanostructures in thermal evaporation method.[23]

A high yield of ZnO nanostructures was obtained by controlling the flow rates and partial pressures of Ar with wet O_2 (Ar/O_2, 350 sccm), and growth temperature was observed at 800 °C.

XRD was used to study the crystalline structure to further understand the influence of morphology variations on the properties of the nanostructures. Figures 5(a)–5(c) show the XRD patterns of the ZnO nanostructures with indexed peaks for assessment of their structure and phase purity grown on three kinds of substrates: (a) Si substrate, (b) PS/Si substrate, and (c) quartz substrate. All nanostructures grown on the Si (100), PS/Si, and quartz substrates were shown to be ZnO polycrystalline with hexagonal structure. The diffraction peaks in the pattern were indexed as the hexagonal wurtzite ZnO structure with lattice constants in accordance with the values in the standard card (JCPDS number 36-1451 for ZnO). The measured lattice parameters ($a = 0.326$ nm and $c = 0.521$ nm) were consistent with the standard values.

The dominant (002) peak for samples (a), (b), and (c) indicates that the *c*-axis of the ZnO nanostructure nanorods, hair-like ZnO NWs, and tetrapod-like rods on the Si, PS/Si, and quartz substrates, respectively, in these samples was perpendicular to the substrate. In addition, the (002) peak intensity for the sample synthesized on quartz was found to be much higher than those of the samples deposited on the Si and PS/Si substrates. Depositing high-quality ZnO nanostructure directly on Si (100) was difficult because of the large lattice mismatch between the ZnO crystal and Si (100). However, no lattice match was assumed for the amorphous glass, which may have been caused by the fewer amounts of ZnO nanostructures grown on the Si substrate than those on the quartz and PS/Si substrates. The effects of the substrates on the structure and morphology of the ZnO nanostructures may be explained by the nucleation and growth process.[23]

The structure and morphology of the ZnO nanostructures were, to a large extent, influenced by the initial number of nuclei formed, which continued to grow and form nanorods and NWs. The major differences among the substrates lie in the lattice structure, defects, and surface chemistries of the substrate surface, which were considered important factors in nucleation and growth.[24] In addition, Deng *et al.*[25] concluded that film crystal orientation is not affected by the crystallographic structure of a substrate. The orientation is a result of a self-ordering effect caused by the minimization of the crystal surface free energy and by the interaction between the deposited material and the substrate surface. Furthermore, the strong intensity and narrow width of the ZnO diffraction peaks also indicate that the resulting products had good crystallinity.

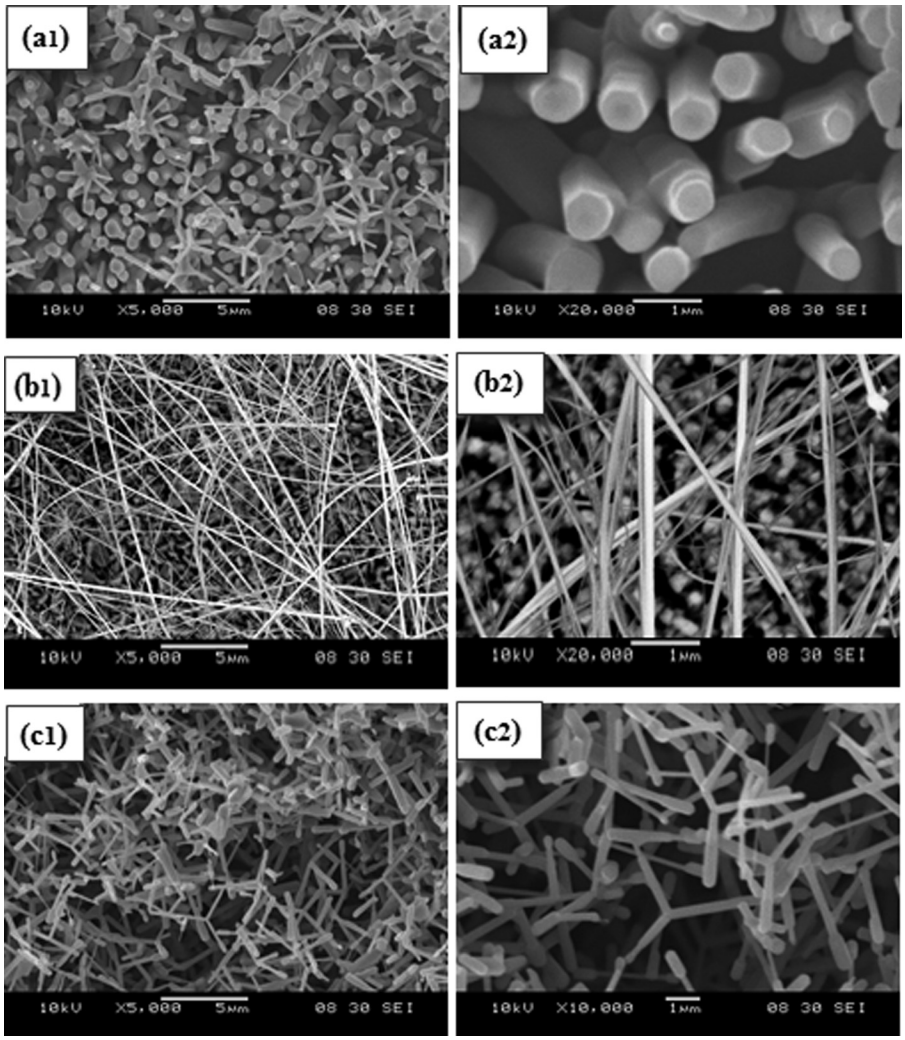

FIG. 4. (a_1) Low and (a_2) high magnification SEM images of ZnO nanorods on Si substrate; (b_1) low and (b_2) high magnification SEM images of hair-like ZnO nanowires grown on PS/Si substrate; (c_1) low and (c_2) high magnification SEM images of tetrapod-like ZnO nanorods grown on quartz substrate.

B. Optical properties

Figures 6(a)–6(c) show the PL spectra of the ZnO nanostructures that were grown on different substrates under the same conditions at room temperature. The higher blue shift luminescence observed in comparison with the energy gap of bulk ZnO (usually, ZnO exhibits a UV emission of ~380 nm) is increased based on surface state, as shown in Table I. The broadening of the bandgap energy occurs with the decrease in the crystallite size. Our results showed that a higher blue shift luminescence is attributed to charge carrier quantum confinement. This indicates that the particles are confined in a lower dimension, and the probability of the

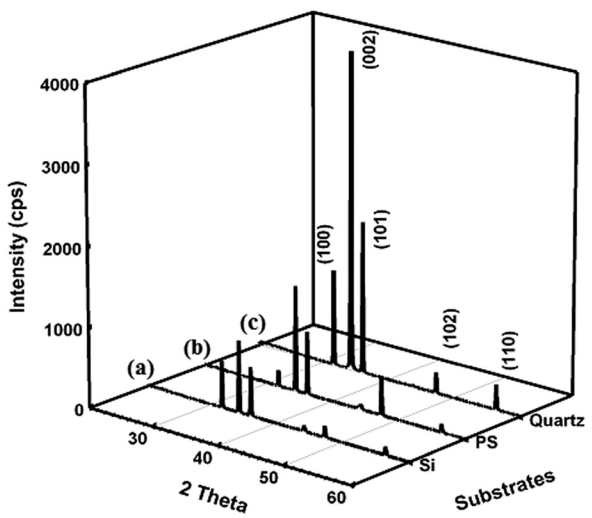

FIG. 5. XRD patterns of the prepared ZnO nanostructures: (a) ZnO nanorods grown on Si substrate, (b) hair-like ZnO nanowires grown on PS/Si substrate, and (c) tetrapod-like ZnO nanorods grown on quartz substrate.

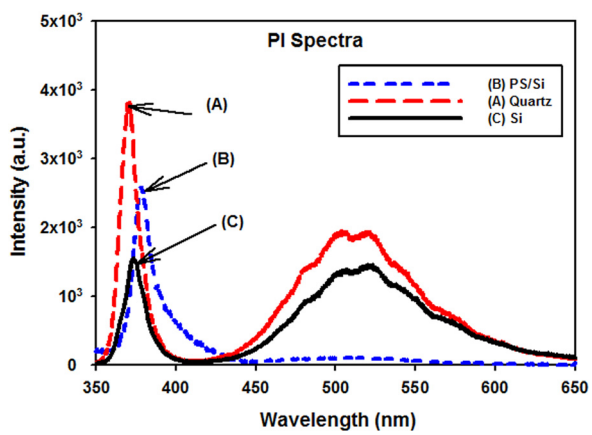

FIG. 6. PL spectra of ZnO nanostructures grown on (a) quartz, (b) PS/Si, and (c) Si substrates at room temperature.

TABLE I. The energy gap, the full width half maximum FWHM, peak shift, intensity, and the radius of nanocystillites of different substrates obtained from the PL spectra at room temperature.

Substrates	Peak position (nm)	FWHM (nm)	Peak shift (nm)	Energy gap (eV)	Nanocrystillites radius (nm)	UV/DLE ratio
Si	374	15.2	6	3.31	5.8	1
PS/Si	378	13.2	2	3.27	4.4	25
Quartz	372	14.1	8	3.33	7.1	2

recombination of the electrons and holes is higher in low-dimensional structures. This state leads to high emission efficiency from the substrates caused by quantum confinement effects. Reducing the dimensions to nanometers drastically changes the physical properties of ZnO structure.

The peak intensity and peak position of the UV emission varied among the ZnO nanostructures grown on the three substrates. Two distinct peaks were observed in PL spectra, the sharp near band-edge emission (NBE), and the broad deep-level emission (DLE) location at ~520 nm. The UV emission corresponds to the NBE emission or the recombination of free excitons through an exciton-exciton collision process[26,27] (at room temperature) caused by NBE electron transition.[28]

All PL spectra showed a strong intensity UV peak at 374, 378, and 372 nm which correspond to Si (nanorods), PS/Si (hair-like NWs), and quartz (tetrapod-like nanorods) substrates, respectively. On the other hand, we found that the green emission DLE peaks at 520 nm in the visible region for the Si and quartz samples had a higher DLE peak as compared with the PS/Si sample. However, the exact origin of the green emission is still in dispute; some authors believed that the green emission bands could be related to the transitions of electrons from shallow donors to Zn vacancies.[29,30] However, some authors may relate the green emission to the native point defects such as V_O or V_{Zn} and suggested as an origin of green PL.[31,32] In fact, the concentrations of the Zn and O vapors can be increased using this method; therefore, the zinc vacancy can be manipulated in such set-up.[27] The full-width half-maximum values of the UV peak were 15.2 nm for the Si substrate, 13.2 nm for the PS/Si substrate, and 14.1 nm for the quartz substrate.

The ratio of the UV to the DLE peak is one of the main factors used to compare the optical properties among samples. The UV/DLE ratio peak for the PS/Si substrate was approximately 1:25, whereas for quartz and Si, their ratios were approximately 1:2 and 1:1, as summarized in Table I. Therefore, the optical quality of the PS/Si hair-like NWs substrate was higher than that of the Si nanorods and quartz nanotetrapods. The UV emission was more intense in NWs with a small aspect ratio, whereas the DLE emission on the PS/Si substrate was dominant in NWs with large aspect ratios.

Based on the quantum confinement luminescence model, the shorter peak wavelength of luminescence is caused by an increase in bandgap energy of the type of substrate materials. This fact indicates that the intensity of the PL is proportional to the number of photons emitted by the surface of materials. A higher energy is dominated by surface-state recombinations, and a low-energy emission originates from the quantum confinement effect.

An approximate size of the ZnO nanostructure required to produce PL can be obtained using the effective mass theory. Assuming infinite potential barriers, the energy gap E for the three-dimensional confined ZnO was obtained as[31]

$$E = E_g + \frac{h^2}{8d^2}\left(\frac{1}{m_e^*} + \frac{1}{m_h^*}\right), \tag{1}$$

where E_g is the bulk ZnO energy gap ($E_g = 3.37$ eV), d is the diameter of the radius of the nanostructure (or the spherical particle), and m_e^* (0.27 m_o), and m_h^* (0.59 m_o) are the electron and hole effective mass for ZnO, respectively.[27] Consequently, Eq. (1) can be used to calculate the values of the radius of ZnO nanostructures from the observed PL peaks: 5.8, 4.4, and 7.1 nm for the Si, PS/Si, and quartz substrates, respectively.

C. Electrical characteristics

Figure 7 shows the *I–V* characteristics of the fabricated ZnO MSM UV photodetectors at 5 V with Pd electrodes grown on different substrates in the dark and under UV illumination. As seen in Fig. 7, the *I–V* curves have been redrawn on a logarithmic scale. For photocurrent measurements, the peak wavelength of the excitation light source was 365 nm, and the incident optical power was 4 W. All samples were annealed at 400 °C for 5 min under N_2 flow. Under a 5 V bias applied after annealing, the dark currents were found to be 2.1×10^{-6}, 2.2×10^{-6}, and 3.08×10^{-7} A, and the UV currents were 4.43×10^{-4}, 7.32×10^{-4}, and 2.65×10^{-5} A for the ZnO photodetectors on the Si, PS/Si, and quartz substrates, respectively.

Furthermore, the contrast ratio of the photocurrent to the dark current was calculated. The value was found to be 210, 333, and 86 times for the three detectors on the Si, PS/Si, and quartz substrates, respectively. In other words, a much higher contrast ratio of photocurrent to dark current from the ZnO MSM photodetector for the ZnO nanowires grown on PS/Si substrate was achieved.

The Schottky barrier height (SBH) of the fabricated devices can be derived from the *I–V* curves. The SBH ϕ_B and ideality factor n were determined using the thermionic emission equation[33]

$$I = I_o\left[\exp\left\{\frac{qV}{nKT}\right\} - 1\right], \tag{2}$$

$$I_o = A^* A T^2 \exp\left\{-\frac{q\phi_B}{kT}\right\}, \tag{3}$$

where I_o is the saturation current based on thermionic emission theory, n is the ideality factor, k is Boltzmann's

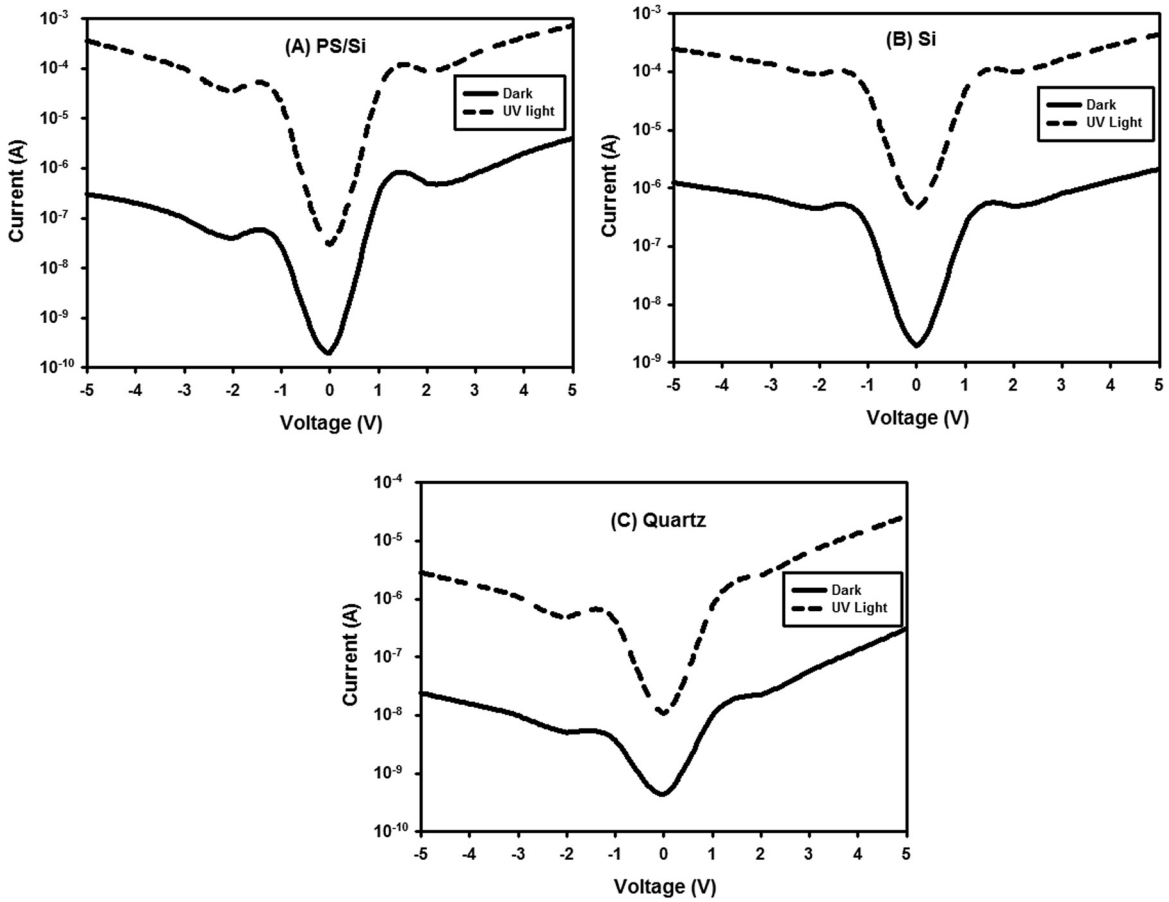

FIG. 7. Current-voltage I-V characteristics for (a) ZnO hair-like nanowire grown on PS/Si substrate, (b) ZnO nanorods grown on Si substrate, and (c) ZnO tetrapod-like nanorods grown on quartz glass substrate photodetector under UV and in dark environment.

constant, T is the absolute temperature, A^* is the effective Richardson coefficient, and ϕ_B is the barrier height. In the equation, the theoretical value of the effective Richardson coefficient of ZnO is $A^* = 32\ \mathrm{A/cm^2\ K^2}$,[34] and thus A^* can be calculated as shown in Eq. (3).

$$A^* = \frac{4\pi m^* q k^2}{h^3}, \tag{4}$$

where h is Planck's constant and $m^* \approx 0.27 m_o$ is the effective electron mass of ZnO,[35] with a contact area of $1.5 \times 10^{-4}\ \mathrm{cm^2}$. Using Eq. (2) and the theoretical value of A^*, the SBHs derived using the I–V method were 0.903, 0.844, and 0.883 eV for the devices based on ZnO nanostructures on Si, PS/Si, and quartz, respectively, in the dark condition. On the other hand, the effective barrier heights under the UV illumination condition were found to be 0.774, 0.704, and 0.800 eV for the samples on Si, PS/Si, and quartz, respectively. The ideality factor values for the fabricated devices were found to increase from 1.2 to 1.6 under UV light and decrease from 1.5 to 1.1 in the dark, which indicates that some non-thermionic processes also contribute to the conduction.[36] Based on Table II, the photodetector samples exhibited more significant changes to the UV light current than that to the dark current characteristics. From these devices, we obtained measurements for an individual ZnO structure, which indicated that they were almost insulating in the dark, with resistance values of approximately 2.4, 2.3, and 16 MΩ. When the samples were exposed to 365 nm UV light, their resistance were remarkably reduced to 11.3, 6.8,

TABLE II. Ideality factor (n), barrier height (φ_B), current at 5 V (A), contrast ratio at 5 V, leakage current at −1 V, and resistance at 5 V for Si (100), PS/Si, and quartz.

Samples (photodetectors)		Ideality factor (n)	Barrier height φ_B (eV)	Current at 5 V (A)	Contrast ratio at 5 V	Leakage current (A) at −1 V	Resistance (R) at 5 V
Si (100)	Dark	1.2	0.903	2.1×10^{-6}	210	2.1×10^{-7}	2.4 MΩ
	UV	1.4	0.774	4.43×10^{-4}		4.3×10^{-5}	11.2 kΩ
PS/Si	Dark	1.1	0.844	2.2×10^{-6}	333	2.7×10^{-8}	2.3 MΩ
	UV	1.2	0.704	7.32×10^{-4}		2×10^{-5}	6.8 kΩ
Quartz	Dark	1.5	0.883	3.1×10^{-7}	86	3.7×10^{-9}	16 MΩ
	UV	1.6	0.800	2.65×10^{-5}		4.2×10^{-7}	188.6 kΩ

and 188 kΩ on Si, PS/Si, and quartz, respectively, as shown in Table II.

In a typical experiment, Kind and coworkers[20] first found that the conductance of ZnO NWs are extremely sensitive to UV light exposure. The light-induced conductivity enabled them to reversibly switch the NWs between off and on states.

Figure 8 show the responsivity as a function of wavelength for the ZnO MSM UV sensors with Pd contact. Spectral responsivity was also measured using a 2 mW xenon arc lamp as light source and a monochromator with light wavelength of 320 nm at 5 V applied bias. Thus, we calculated the responsivity from $\left(R = \frac{I_{ph}}{p_{inc}}\right)$, where (R) is the responsivity of the detectors, (I) is the photocurrent (in A), and (P_{inc}) is the power of the xenon arc lamp (in W). The photodetector responsivities were found to be nearly constant below the bandgap UV region (300–380 nm), whereas sharp cutoffs with a drop of 3 to 4 orders of magnitude occurred at approximately 390 nm to 420 nm. The maximum responsivities for the fabricated Pd/ZnO/Pd MSM photodetectors on the PS/Si, Si, and quartz substrates were 0.22, 0.073, and 0.053 A/W, respectively. The quantum efficiency of our photodetectors can be calculated by measuring the spectral response via

$$\eta = R \times \frac{hc}{q\lambda} \times 100\%, \tag{5}$$

where η is the quantum efficiency, R is the measured responsivity, q is the electron charge, λ is the incident light wavelength, h is Planck constant, and c is the speed of light.[35,37,38] From Eq. (5), the quantum efficiency values of the Pd/ZnO photodetectors obtained were about 85%, 28.2%, and 20.5% for the PS/Si, Si, and quartz substrates, respectively. From these measurements, the responsivity for the ZnO/PS photodetector was found to be approximately four times higher compared with the ZnO photodetector on the Si and quartz substrates. The responsivity dependence of the photodiodes was attributed to the difference in surface reactivity and/or the defect density on the ZnO substrate surface. These results indicate that high-performance ZnO Schottky photodiodes can be fabricated using ZnO nanowires with higher photosensitivity.

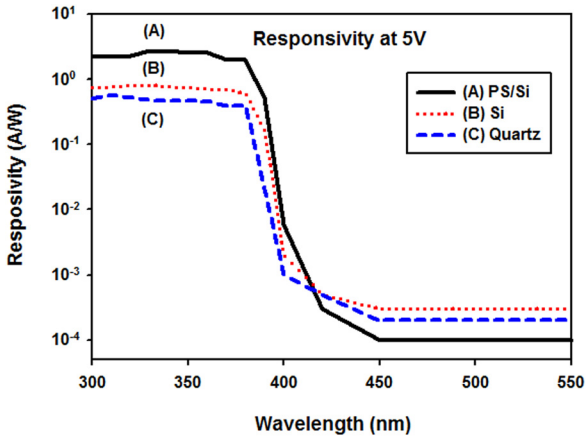

FIG. 8. Responsivity spectra of MSM photodetectors based on (a) ZnO hair-like nanowires grown on PS/Si substrate, (b) ZnO nanorods on Si substrate, and (c) ZnO tetrapod-like nanorods grown on quartz substrates at room temperature under 5 V applied bias.

D. Response time

The optical response of ZnO nanostructures deposited on three different substrates Si, PS/Si, and quartz was studied using dynamic response time measurements. The effects of the substrates were investigated by exposing them to a pulse at 365 nm UV light.

Figures 9(a)–9(c) plots the photoresponse of ZnO nanostructures as a function of time while the UV light was switched on and off at different durations. Photoconductive response is a key figure of merit for a photodetector. The response of the entire UV detector was measured using a 365 nm UV source at a bias of 1 V. The real-time on/off switching was measured by applying a UV pulse with an intensity of 1.5 mW/cm^2. The measured photocurrent for all the detectors showed a rapidly increasing value upon exposure to UV light, and the current decreased in dark conditions. The photodetectors showed much faster switching under pulsed UV illumination for the device on the PS/Si substrate compared with the device on the Si and quartz substrates.

The response time of the ZnO photodetectors to UV exposure was found to be highly dependent on the type of substrates, with a value as high as 2.5 times greater in the case of the PS/Si substrate compared with the Si and quartz substrates. These nanostructures can evidently be reversibly and rapidly switched between low and high conductivity states. The rise and decay times of the fastest NWs switches were below the apparatus detection limit, which was roughly 1 ms.

Furthermore, the ZnO nanowires on PS/Si detector showed fast photoresponse with a rise time of 0.089 s and a fall time of 0.085 s, whereas ZnO nanorods on Si and ZnO nannotetrapods/quartz detectors showed a slow response with rise times of 0.194 and 0.128 s and fall times of 0.4 and 0.362 s, respectively. These results indicate that the nanostructure uniformity of the ZnO nanowires grown on the PS/Si substrate could lead to a fast response time and better UV detection than the ZnO nanorods on Si and nanotetrapods on quartz substrates as illustrated in SEM images and PL measurements. These results confirm that the thermal evaporation method not only provides a simple and a cost effective way to integrate highly photosensitive ZnO nanodevices with conventional circuits without using e-beam lithography techniques and/or additional costly deposition processes but also allows for the fabrication of devices with higher photosensitivity.

E. Mechanism of ZnO NW photodetector

Nanostructures have the advantage of a high surface area, and electronic processes are strongly influenced by surface processes. Because of the high surface-to-volume ratio, trapping-at-surface states drastically affect the transport and photoconduction properties of NWs. As discussed by Soci *et al.*, and other groups,[39] in a dark condition, oxygen molecules are adsorbed on the NW surface and capture free

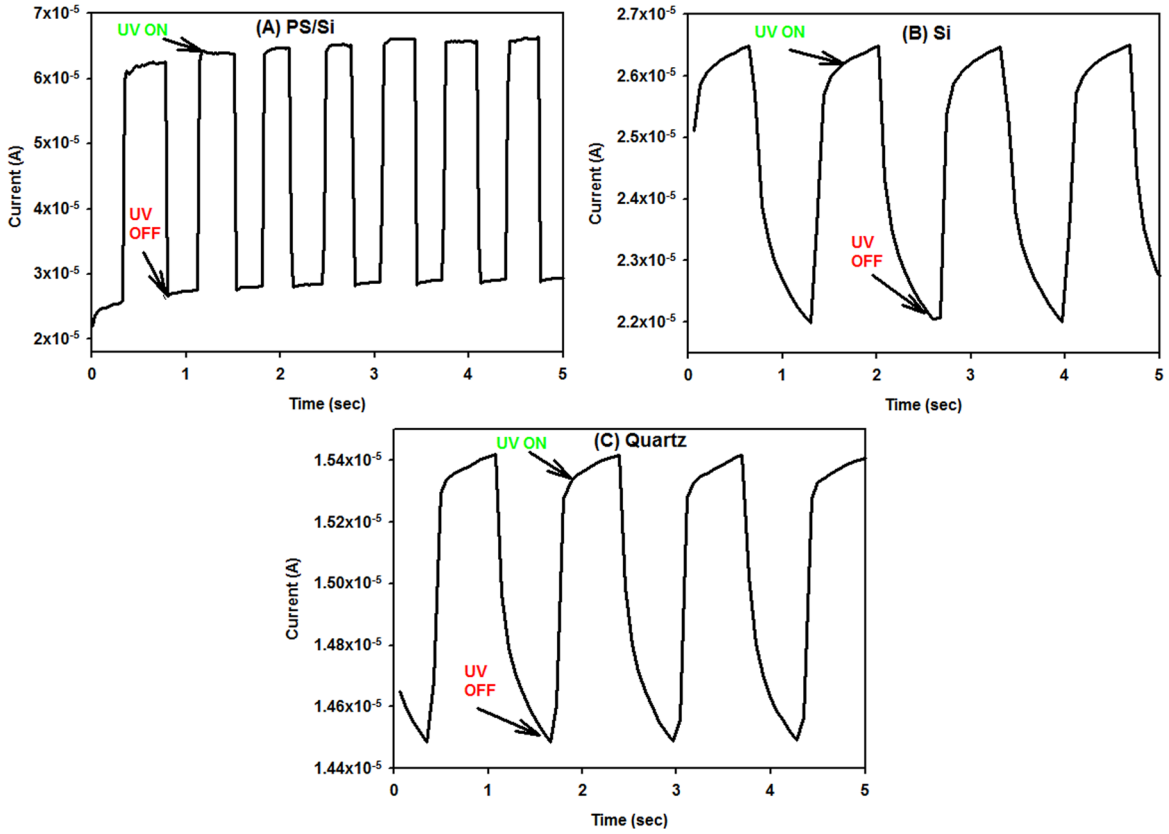

FIG. 9. The photocurrent time response of photodetectors based on (a) ZnO nanowires/PS, (b) ZnO nanorods/Si, and (c) ZnO nanotetrapods/quartz.

electrons from the n-type ZnO. This leads to a build-up of negatively charged O_2 ions on the surface, which creates a low conductivity depletion layer near the NW surface

$$O_2(g) + e^- \rightarrow O_2^-(ad). \quad (6)$$

When the detector is exposed to UV, electron–hole pairs are photo-generated and holes are trapped at the surface by oxygen ions via surface electron–hole recombination

$$h + O_2^- \rightarrow O_2(g). \quad (7)$$

Unpaired electrons are left behind, which add to the photocurrent.[40] Thus, NWs are very suitable for obtaining higher sensitivity of the devices because of an enhanced surface-to-volume ratio. Schottky barrier demonstrates hole-trapping in the reversed bias junction that reduces the depletion region and assists tunneling of additional electrons.[41] The nanostructures can also have potential in optoelectronic switches, with the insulating state as "OFF" state in the dark and the conductance state as "ON" when exposed to UV light. The current rises in the ZnO nanostructures under UV exposure, which can be attributed to the increase in the charge carrier density caused by the introduction of additional photogenerated electrons, together with the lowered barrier height caused by photo-desorption of negatively charged surface oxygen.[42] The current decay upon UV off can then be attributed to chemisorptions of oxygen on the surface of ZnO nanostructures that capture electrons from the ZnO nanorods. Researchers[43–45] previously reported that unlike in all most cases of ZnO NW devices, the current decay process was much slower than the current rise process. The reason for such phenomenon is still unclear.

IV. CONCLUSION

In summary, we have demonstrated that ZnO nanostructures can be synthesized using the thermal evaporation method without using any metal catalyst or a ZnO seed layer that serves as a substitute for the metal catalyst. A variety of high-quality ZnO nanostructures, including nanorods, nanotetrapod, and hair-like NWs, have been synthesized through the VS process using Si (100), quartz glass, and PS/Si substrates, respectively. MSM photodetectors with Pd as contact electrodes have been successfully constructed for UV detection. The ZnO nanowires/PS detector shows the fastest photoresponse with a rise time of 0.089 s and a fall time of 0.085 s, whereas ZnO nanotetrapods/quartz and ZnO NWs/Si show a slow response with rise times of 0.128 and 0.194 s and fall times of 0.362 and 0.4 s, respectively. This detector has very high stability and reliability at a wavelength of 365 nm with repetitive shots. Results indicate that the thermal evaporation method is a simple and a cost-effective way to fabricate devices with higher photosensitivity without using complex techniques.

ACKNOWLEDGMENTS

Support from ERGS grant and Universiti Sains Malaysia is gratefully acknowledged.

[1]X. S. Fang, Y. Bando, U. Gautam, C. H. Ye, and D. Golberg, J. Mater. Chem. **18**, 509 (2008).
[2]M. H. Huang, S. Mao, H. Feick, H. Yan, Y. Wu, H. Kind, E. Weber, R. Russo, and P. Yang, Science **292**, 1897 (2001).
[3]S. W. Kim, Sz. Fujita, and Sg. Fujita, Appl. Phys. Lett. **86**, 153119 (2005).
[4]W. I. Park and G.-C. Yi, Adv. Mater. **16**, 87 (2004).
[5]Z. W. Pan, Z. R. Dai, and Z. L. Wang, Science **291**, 1947 (2001).
[6]H. I. Abdulgafour, Z. Hassan, N. H. Al-Hardan, and F. K. Yam, Physica B **405**, 4216 (2010).
[7]F. Krumeich, H. J. Muhr, M. Niederberger, F. Bieri, B. Schnyder, and R. Nesper, J. Am. Chem. Soc. **121**, 8324 (1999).
[8]X. Wang, C. J. Summers, and Z. L. Wang, Nano Lett. **4**, 423 (2004).
[9]T. Sahoo, E.-S. Kang, M. Kim, V. Kannan, Y.-T. Yu, D.-C. Shin, T.-G. Kim, and I.-H. Lee, J. Cryst. Growth **310**, 570 (2008).
[10]S. Y. Li, P. Lin, C. Y. Lee, M. S. Ho, and T. Y. Tseng, J. Nanosci. Nanotechnol. **4**, 968 (2004).
[11]H. T. Ng, J. Han, T. Yamada, P. Nguyen, Y. P. Chen, and M. Meyyappan, Nano Lett. **4**, 1247 (2004).
[12]Y. Zhang, H. Jia, R. Wang, C. Chen, X. Luo, D. Yu, and C. Lee, Appl. Phys. Lett. **83**, 4631 (2003).
[13]P. Chang, Z. Fan, W. Tseng, D. Wang, W. Chiou, J. Hong, and J. G. Lu, Chem. Mater. **16**, 5133 (2004).
[14]S. Y. Li, C. Y. Lee, and T. Y. Tseng, J. Cryst. Growth **247**, 357 (2003).
[15]C. J. Lee, T. J. Lee, S. C. Lyu, Y. Zhang, H. Ruh, and H. J. Lee, Appl. Phys. Lett. **81**, 3648 (2002).
[16]P. X. Gao, Y. Ding, and Z. L. Wang, Nano Lett. **3**, 1315 (2003).
[17]X. Y. Kong and Z. L. Wang, Nano Lett. **3**, 1625 (2003).
[18]Z. L. Wang, ACS Nano **2**, 1987 (2008).
[19]Z. L. Wang, Annu. Rev. Phys. Chem. **55**, 159 (2004).
[20]H. Kind, H. Q. Yan, B. Messer, M. Law, and P. D. Yang, Adv. Mater. **14**, 158 (2002).
[21]H. I. Abdulgafour, F. K. Yam, Z. Hassan, K. Al-Heuseen, and M. J. Jawad, J. Alloys Compd. **509**, 5627 (2011).
[22]C. Ye, X. Fang, Y. Hao, X. Teng, and L. Zhang, J. Phys. Chem. B **109**, 19758 (2005).
[23]X. D. Yan, Z. W. Li, R. Q. Chen, and W. Gao, Cryst. Growth Des. **8**(7), 2406 (2008).
[24]Y. Sun, N. A. Fox, D. J. Riley, and M. N. R. Ashfold, J. Phys. Chem. C **112**(25), 9234 (2008).
[25]S. Xu, C. S. Lao, B. Weintraub, and Z. L. Wang, J. Mater. Res. **23**(8), 2072 (2008).
[26]L. Vayssieres, Adv. Mater. **15**(5), 464 (2003).
[27]D. G. Zhao, S. J. Xu, M. H. Xie, S. Y. Tong, and H. Yang, Appl. Phys. Lett. **83**(4), 677 (2003).
[28]K. Vanheusden, C. H. Seager, W. L. Warren, D. R. Tallant, and J. A. Voigt, Appl. Phys. Lett. **68**(3), 403 (1996).
[29]Y. W. Heo, D. P. Norton, and S. J. Pearton, J. Appl. Phys. **98**, 073502 (2005).
[30]U. Ilyas, R. S. Rawat, T. L. Tan, P. Lee, R. Chen, H. D. Sun, L. Fengji, and S. Zhang, J. Appl. Phys. **110**, 093522 (2011).
[31]K. Vanheusden, W. L. Warren, C. H. Seager, D. R. Tallant, J. A. Voigt, and B. E. Gnade, J. Appl. Phys. **79**, 7983(1996).
[32]H. I. Abdulgafour, Z. Hassan, F. K. Yam, K. AL-Heuseen, and Y. Yusof, Appl. Surf. Sci. **258**, 461 (2011).
[33]E. H. Rhoderick and R. H. William, *Metal–Semiconductor Contacts*, 2nd ed. (Oxford University Press, New York, 1998).
[34]R. E. Hummel, *Electronic Properties of Materials* (Springer, Berlin, 1992), p. 373.
[35]J. C. Carrano, P. A. Grudowski, C. J. Eiting, R. D. Dupuis, and J. C. Campbell, Appl. Phys. Lett. **70**, 1992 (1997).
[36]S. Y. Lee and S. K. Lee, Nanotechnology **18**, 495701 (2007).
[37]L. Guo, H. Zhang, D. Zhao, B. Li, Z. Zhang, M. Jiang, and D. Shen, Sens. Actuators B **166–167**, 12 (2012).
[38]W. Y. Weng, S. J. Chang, C. L. Hsu, T. J. Hsueh, and S. P. Changa, J. Electrochem. Soc. **157**, K30–K33 (2010).
[39]C. Soci, A. Zhang, B. Xiang, S. A. Dayeh, D. P. R. Aplin, J. Park, X. Y. Bao, Y. H. Lo, and D. Wang, Nano Lett. **7**, 1003 (2007).
[40]L. J. Mandalapu, F. Xiu, Z. Yang, and J. Liu, Mater. Res. Soc. Symp. Proc. **891**, 1–6 (2006).
[41]R. R. Mehta and B. S. Sharma, J. Appl. Phys. **44**, 325 (1973).
[42]Y. W. HeO, D. P. Norton, L. C. Tien, Y. Kwon, B. S. Kang, F. Ren, and S. J. Pearton, Mater. Sci. Eng. **R47**, 1–47 (2004); available online http://dx.doi.org/10.1016/j.mser.2004.09.001.
[43]S. E. Ahn, J. S. Lee, H. Kim, S. Kim, B. H. Kang, K. H. Kim, and G. T. Kim, Appl. Phys. Lett. **84**(24), 5022 (2004).
[44]Q. H. Li, Y. X. Liang, Q. Wan, and T. H. Wang, Appl. Phys. Lett. **85**(26), 6389 (2004).
[45]Z. Fan, P. C. Chang, J. G. Lu, E. C. Walter, R. M. Penner, C. H. Lin, and H. P. Lee, Appl. Phys. Lett. **85**(25), 6128 (2004).